

The role of climate-driven chemical weathering on soil production

Kevin P. Norton^{a,*}, Peter Molnar^b, Fritz Schlunegger^c

^a School of Geography, Environment and Earth Sciences, Victoria University of Wellington, New Zealand

^b Institute of Environmental Engineering, ETH Zurich, Switzerland

^c Institute of Geological Sciences, University of Bern, Switzerland

ARTICLE INFO

Article history:

Received 11 February 2013

Received in revised form 21 August 2013

Accepted 25 August 2013

Available online 4 September 2013

Keywords:

Soil production function

Soil depth

Numerical modelling

Weathering limits

ABSTRACT

Climate plays an important role in controlling rates of weathering and weathered regolith production. Regolith production functions, however, seldom take climate parameters into account. Based on a climate-dependent weathered regolith production model, at low denudation rates, relative regolith thicknesses are less sensitive to changes in precipitation rates, while at high denudation rates, small changes in climatic parameters can result in complete stripping of hillslopes. This pattern is compounded by the long residence times and system response times associated with low denudation rates, and vice versa. As others have shown, the transition between regolith-mantled and bedrock slopes is dependent on the ratio of denudation to production. Here, we further suggest that this is itself a function of precipitation rate and temperature. We suggest that climatic parameters can be easily incorporated into existing soil production models and that such additions improve the predictive power of soil production models.

© 2013 Elsevier B.V. All rights reserved.

1. Introduction

1.1. Modelling soil formation for timescales spanning thousands of years

Hillslopes comprise the entire range of landscapes, from thick soil mantles to bare rock. Soil thickness on these slopes is a function of upbuilding and downwasting processes including incorporation of organic material, aeolian deposition and compaction among others (Johnson et al., 2005a,b). The mechanisms and rates of regolith production on hillslopes and the formation of soils have been addressed in numerical studies, mainly through the use of depth-decay functions where weathering rates decay exponentially with increasing soil thickness (e.g., Tucker and Slingerland, 1994; Heimsath et al., 1997; Tucker and Slingerland, 1997), or by hump-shaped functions (Humphreys and Wilkinson, 2007; Heimsath et al., 2009; Pelletier and Rasmussen, 2009; Gabet and Mudd, 2010) where weathering rates are at their maximum for a limited soil thickness, which is commonly 20–40 cm. Despite the wealth of soil production data, there has been little headway made towards integrating climate into soil production models. Pelletier and Rasmussen (2009) presented a climate-dependent weathering model

based on effective energy and mass transfer (EEMT; Rasmussen and Tabor, 2007):

$$EEMT = 347,134e^{-1/2 \left[\left(\frac{MAT-21.5}{-10.1} \right)^2 + \left(\frac{MAP-4412}{1704} \right)^2 \right]} \quad (1)$$

$$P_0 = ae^{bEEMT} \quad (2)$$

where *MAT* is the mean annual temperature in °C, *MAP* is the mean annual precipitation in mm yr⁻¹, *a* (m ky⁻¹) and *b* (m² kJ⁻¹ yr⁻¹) are empirically derived constants, and *P*₀ is the bedrock lowering rate (m ky⁻¹). This model does a good job of predicting weathered regolith production rates in the tested settings (data from Riebe et al., 2004). The EEMT model is effective, but does not directly address primary mineral weathering. While soil production and weathering are not interchangeable, the weathering of primary minerals is a vital step in the production of most soils, especially for regions where inputs through colluvial, alluvial, or aeolian sources are lacking (Minasny et al., 2008). Mineral-specific weathering and regolith production models have been developed in the past few years (Ferrier and Kirchner, 2008; Lebedeva et al., 2010). These models have been instrumental in identifying the boundaries between supply limited and kinetically-limited weathering, but they do not explicitly include climate variables such as precipitation. Two recent papers (Dixon and von Blanckenburg, 2012; Heimsath et al., 2012) have come to slightly different conclusions with respect to the limits on soil production. Dixon and von Blanckenburg (2012) suggest a global maximum soil production rate (dependent on lithology) while Heimsath et al. (2012) build on the concept that the maximum

* Corresponding author. Tel.: +64 4463 6993.

E-mail address: kevin.norton@vuw.ac.nz (K.P. Norton).

production rate is also dependent on erosion rates such that faster erosion rates yield faster regolith production rates. Important in these studies is the consideration that soil formation and weathering are ultimately linked for geomorphic time scales spanning thousands to hundred thousands of years, which we build on here.

In this paper, we use a climate-dependent model of regolith production that can be easily introduced into landscape evolution models. Our model is based on existing geomorphic transport laws (Dietrich et al., 2003) and weathering equations (White and Blum, 1995) operating on hillslopes, and includes precipitation, temperature, and erosion rate as independent variables. Dixon and von Blanckenburg (2012) defined regolith production as the chemical alteration of bedrock to form saprolite, and soil production as the disturbance of saprolite to create soil. We address the simplest case where soil is formed directly from bedrock weathering. Likewise, we consider a simple scenario in which soil thickness reaches a steady state related to weathering and erosion. While this assumption may not hold for all natural settings, some locations display relatively simple soil production functions which are dependent on soil thickness and potentially erosion rate (Heimsath et al., 1997). In this case, regolith production and soil production are equivalent. As such, soil production in this model is accomplished through the chemical alteration of primary silicate minerals. We note that processes such as bedrock cracking through physical processes, formation of weathering pathways, lithological heterogeneities and orientation of geological fabric are boundary conditions with important consequences for weathering rates. However, we explicitly focus on this simple end member scenario to explore the extent to which climate-controlled chemical alteration contributes to the formation of soils and weathering covers, how these mechanisms compete with surface erosion, and how hillslopes respond if thresholds in weathering and erosion ratios are reached.

1.2. Rates of soil formation

Soil mantled slopes are formed in those landscapes where hillslope transport rates are slower than the weathering rates of bedrock. The resulting hillslopes display smooth curvatures, and the unconsolidated material is often transferred in the downslope direction by diffusive style processes, such as soil creep (e.g., Roering et al., 1999). In contrast, in landscapes where hillslope transport rates or fluvial incision rates exceed the upper limit of bedrock weathering rates, bedrock becomes exposed on hillslopes. These landscapes transport material to streams by episodic mass failure such as rock avalanches and landsliding. These mechanisms have been associated with large variations in denudation rates. Diffusive soil creep typically occurs at rates below 0.2 mm yr^{-1} (Binnie et al., 2007; DiBiase et al., 2010; Norton et al., 2010), while stochastic mass wasting is associated with order of magnitude faster denudation rates (Binnie et al., 2007; DiBiase et al., 2010; Norton et al., 2010; Savi et al., in press). Erosion rates on soil-covered hillslopes have been measured using in situ produced cosmogenic ^{10}Be , ^{26}Al , and ^{21}Ne concentrations in bedrock sampled under soils of different depths. The rates range from $\sim 0.06\text{--}0.38 \text{ mm yr}^{-1}$ for the central European Alps (Norton et al., 2008, 2010), $\sim 0.08\text{--}0.37 \text{ mm yr}^{-1}$ in the western United States (Heimsath et al., 1997, 2001a, 2005), $0.05\text{--}0.14 \text{ mm yr}^{-1}$ in western Australia (Heimsath et al., 2000, 2001b), ca. 0.2 and 0.05 mm yr^{-1} for soil-mantled hillslopes in northern Peru and northern Chile, respectively (Kober et al., 2006; Abbühl et al., 2010), and to 0.03 mm yr^{-1} in the Appalachian Mountains (Matmon et al., 2002). Cosmogenic nuclide-derived denudation rates in these settings average over $\sim 10^4\text{--}10^5 \text{ yr}$ timescales, which is long enough to integrate diffusive processes on soil mantled hillslopes. Episodic erosion rates are typically an order of magnitude faster, measuring $1\text{--}3 \text{ mm yr}^{-1}$ in the western United States (Binnie et al., 2007), $>3 \text{ mm yr}^{-1}$ in the Swiss Alps (Norton et al., 2010), and $2\text{--}4 \text{ mm yr}^{-1}$ in the Italian Alps (Savi et al., in press). These rates average over $\sim 10^3$ years, similar to the

recurrence intervals for stochastic mass failure. Accordingly, the presence or absence of a soil cover on hillslopes is a key indicator of long-term erosion rates, and for the interpretation of possible erosional mechanisms in a landscape.

2. Modelling approach

2.1. Regolith production on hillslopes

We are primarily interested here in modelling the production of regolith on hillslopes under variable climate parameters. We explicitly determine regolith production rates and thicknesses assuming the system approaches a steady state. In particular, in the absence of profile collapse or inflation, mass balance on the hillslope requires that;

$$\frac{dH}{dt} = SPR - D \quad (3)$$

where H is the soil depth (L), SPR is the soil production rate (L T^{-1}), and D is the total denudation rate (L T^{-1}) – see Tucker and Hancock (2010) for a complete review of continuity of mass equations.

The denudation rate term is more fully expressed as the sum of the physical erosion rate and chemical weathering rate. However, the combined denudation term has the advantage of being directly quantifiable at the hillslope to catchment scale. In particular, cosmogenic nuclide-derived denudation rates are available for catchments around the world (see von Blanckenburg (2006) for review), and therefore make a convenient model input. The implications of this assumption are discussed below.

The remaining term on the right side of Eq. (3) is regolith production. Measurements of weathered regolith production rates are less common. Where they have been measured or estimated, rates tend to be between $\sim 10^{-4}$ and $10^{-5} \text{ m yr}^{-1}$ (Heimsath et al., 1997, 2000, 2001a,b; Bierman and Nichols, 2004; Heimsath et al., 2005; Norton et al., 2008, 2010) depending on lithology and climate. This production rate is also dependent on the thickness of regolith, and is commonly modelled using an exponential depth dependent function (e.g., Ahnert, 1967):

$$SPR = SPR_{\max} e^{-\alpha H} \quad (4)$$

where SPR_{\max} is the maximum soil production rate under zero regolith cover (L T^{-1}), and α is a rate constant (L^{-1}) (Table 1). The parameters SPR_{\max} and α have been determined by Heimsath et al. (1997, 2000, 2001a,b, 2005) to range between $\sim 5 \times 10^{-5}$ and $3.7 \times 10^{-4} \text{ m yr}^{-1}$ and 1.7 and 4 m^{-1} , respectively, for a range of granitic and quartz-bearing sedimentary rocks. The value of α for granitic rocks is typically $\sim 2 \text{ m}^{-1}$ (Heimsath et al., 2000, 2005).

While the exponential production function has been shown to perform well in some landscapes (e.g., Heimsath et al., 1997, 2000, 2001a,b, 2005), a “humped” regolith production function has also been observed in nature (Heimsath et al., 2009). The hump-shaped function exhibits a maximum production rate under a thin soil cover (Carson and Kirkby, 1972; Ahnert, 1976; Anderson, 2002). Here, we use the approach of Anderson (2002) and Pelletier and

Table 1
Model inputs.

a_0	0.42	Best fit to Riebe et al. (2004)
E_a	77 kJ mol^{-1}	White and Blum (1995)
α	3 m^{-1}	Best fit to Riebe et al. (2004)
T_0	278.15 K	White and Blum (1995)

Rasmussen (2009) and describe the hump-shaped function as a combination of a linear increase followed by an exponential decrease with depth:

$$SPR = SPR_{\max} e^{-\frac{H}{h_0}} \text{ for } H > 0.6h_0 \quad (5)$$

$$SPR = 0.9SPR_{\max} \frac{H}{h_0} \text{ for } H \leq 0.6h_0 \quad (6)$$

where h_0 is the characteristic regolith depth at which soil production is maximised, ranging from ~0.2 and 0.4 m (Anderson, 2002; Gabet and Mudd, 2010), and is related to the rate constant α of the exponential model in Eq. (4), i.e., $\alpha = 1 / h_0$.

Here, we assume that the maximum production rate can be scaled by climate parameters, analogous to the scaling of chemical fluxes (White and Blum, 1995). While this admittedly focuses on solely the chemical component of weathering, Gabet and Mudd (2010) showed that a hump-shaped production function can arise from a purely physically-based disturbance model. We therefore indirectly include physical processes of erosion by modelling regolith production with a hump-shaped model. We justify our approach on the basis that, in the case of steady state, the rate of regolith formation is equal to the rate of denudation at the surface, or equally, the sum of physical erosion and chemical weathering. This implies a direct link between the rate of chemical weathering and the rate of regolith formation. Accordingly, the process of regolith formation, in its simplest form, involves the dissolution of primary minerals and precipitation of secondary minerals. We note that this precludes processes such as clay mineral transformation and inflation, which can contribute substantially to some soils (Jenny, 1941). To this end, we use a modified Arrhenius formula suggested by White and Blum (1995) and used by Dixon et al. (2009) for the dependence of chemical weathering on temperature and precipitation:

$$SPR_{\max} = a_0 P e^{-\frac{E_a}{R} \left(\frac{1}{T} - \frac{1}{T_0} \right)} \quad (7)$$

where a_0 scales the precipitation rate P ($L T^{-1}$) to the regolith production function (similar to the A_i of White and Blum, 1995) accounting for a regolith bulk density $\rho = 1600 \text{ kg m}^{-3}$, E_a is the average activation energy for silicate mineral weathering, here taken to be 77 kJ mol^{-1} (Velbel, 1993; White and Blum, 1995), R is the gas constant, T is the temperature (in K) and T_0 is a reference temperature (in K) usually assumed to be 5°C . Such temperature dependence is regularly seen in weathering systems (White and Blum, 1995; Egli et al., 2003; Dixon et al., 2009; Williams et al., 2010). A more complete model would include the entire soil water flux including precipitation, evapotranspiration, and infiltration rates (Volobuyev, 1974). However, the actual soil and ground-water fluxes are often unknown. We, therefore, use annual precipitation as a proxy for the total water potentially available for weathering.

Substituting Eqs. (4) and (7) into Eq. (3) gives the change in regolith depth with time as a function of temperature, precipitation, and denudation for the exponential function;

$$\frac{dH}{dt} = a_0 P e^{-\frac{E_a}{R} \left(\frac{1}{T} - \frac{1}{T_0} \right)} e^{-\alpha H} - D \quad (8)$$

The climate-denudation dependent hump-shaped regolith production function results from substituting Eqs. (5) to (7) into Eq. (3).

$$\frac{dH}{dt} = a_0 P e^{-\frac{E_a}{R} \left(\frac{1}{T} - \frac{1}{T_0} \right)} e^{-\frac{H}{h_0}} - D \text{ for } H > 0.6h_0 \quad (9)$$

$$\frac{dH}{dt} = 0.9a_0 P e^{-\frac{E_a}{R} \left(\frac{1}{T} - \frac{1}{T_0} \right)} \frac{H}{h_0} - D \text{ for } H \leq 0.6h_0 \quad (10)$$

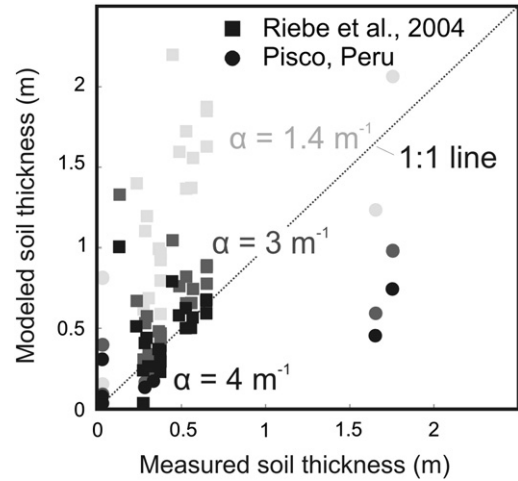


Fig. 1. Calibration of the model using the Riebe et al.'s (2004) data ($R^2 = 0.78$, $p < 0.05$) and data for the Rio Pisco, Peru ($R^2 = 0.16$, $p = 0.38$). The best fit for all data is for $\alpha = 3 \text{ m}^{-1}$ ($R^2 = 0.60$, $p < 0.01$); however, significant fits can also be calculated for $\alpha = 1.4\text{--}4 \text{ m}^{-1}$.

Eqs. (8) to (10) express variations in regolith thickness in terms of three partially independent variables: D , which can be measured using cosmogenic nuclides (see Section 1.2), T and P . The strong dependence of regolith thickness on precipitation and denudation is supported by recent work by Rasmussen et al. (2011) in which they show first order controls on weathering rates by both water availability and erosion rate. To investigate response times and sensitivity, we solve Eqs. (8) to (10) stepwise from a starting soil thickness of 0 for the exponential form and 10 cm for the hump-shaped form, and run them to steady state.

Each of these equations can be solved for the steady state regolith thickness ($dH / dt = 0$) for a given combination of denudation and climate parameters:

$$H = -\frac{1}{\alpha} \ln \left(\frac{D}{a_0 P e^{-\frac{E_a}{R} \left(\frac{1}{T} - \frac{1}{T_0} \right)}} \right) = -h_0 \ln \left(\frac{D}{a_0 P e^{-\frac{E_a}{R} \left(\frac{1}{T} - \frac{1}{T_0} \right)}} \right) \quad (11)$$

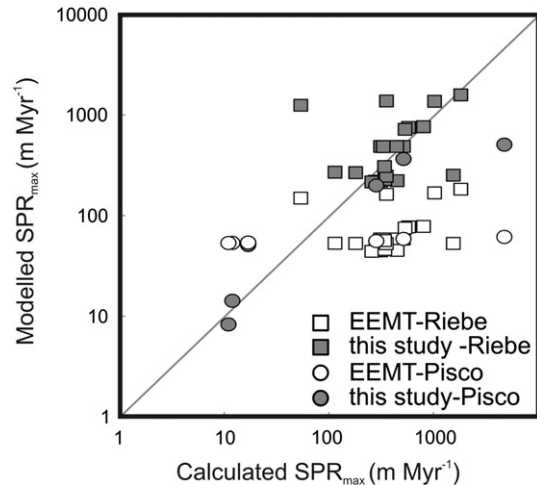


Fig. 2. Modelled maximum soil production rates (SPR_{\max}) using the EEMT method (Pelletier and Rasmussen, 2009; exponential, $R^2 = 0.09$, $p = 0.09$) and the silicate dissolution model (this paper; exponential, $R^2 = 0.1$, $p = 0.09$) versus maximum soil production rates. SPR_{\max} is calculated from soil depth and denudation rates measured by Riebe et al. (2001, 2004) and in the Rio Pisco, Peru, assuming steady state soil thickness and an exponential soil production function (cf. Heimsath et al., 1997).

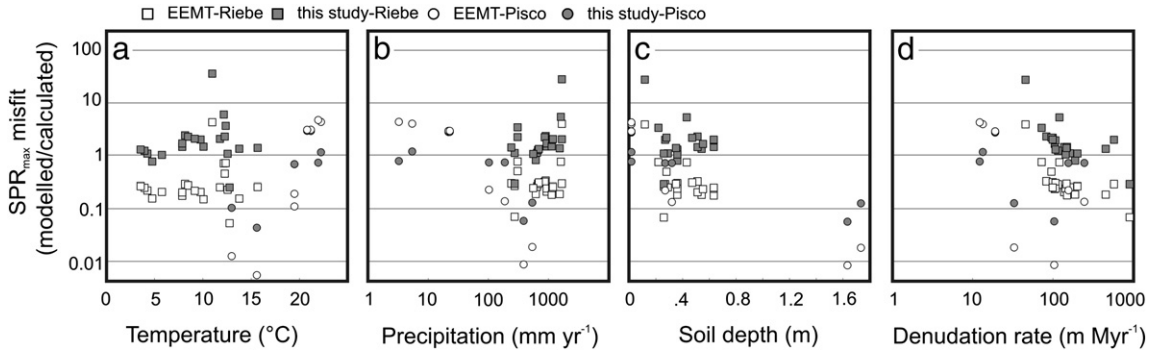


Fig. 3. Model misfits for a) temperature, b) precipitation, c) soil depth, and d) denudation rates. For the *EEMT* model, gradients are apparent for both temperature and precipitation as well as soil depth. For the silicate weathering model, misfits tend to be randomly distributed. In the case of the Rio Pisco data, both models predict lower SPR_{max} at higher denudation rates. This may be explained if SPR_{max} is denudation rate dependent (i.e., Heimsath et al., 2012).

in the exponential case, and:

$$H = -h_0 \ln \left(\frac{D}{a_0 P e^{-\frac{\alpha}{R} \left(\frac{1}{T} - \frac{1}{T_0} \right)}} \right) \quad \text{for } H > 0.6h_0 \quad (12)$$

$$H = \frac{h_0 D}{0.9 a_0 P e^{-\frac{\alpha}{R} \left(\frac{1}{T} - \frac{1}{T_0} \right)}} \quad \text{for } H \leq 0.6h_0 \quad (13)$$

for the hump-shaped function.

The model requires an estimate of a_0 that scales P to the soil production function, and α that is a rate constant for the soil production rate function. We proceeded using data from Riebe et al. (2001, 2004), discounting all denudation rates and regolith depths which were averaged or estimated, and those from the Rio Pisco, Peru, to calibrate the model.

3. Results

3.1. Model calibration and misfits

The resulting best fit for the data gives $a_0 = 0.42$ and $\alpha = 3 \text{ m}^{-1}$ ($R^2 = 0.78$, $p < 0.05$; Fig. 1) for temperature in K, precipitation in mm, denudation and regolith production rates in $\text{t km}^{-2} \text{ yr}^{-1}$ and depth in m. Denudation and production rates are consistently converted to linear units (m Myr^{-1}) using 1600 and 2700 kg m^{-3} for regolith and bedrock densities, respectively. Significant correlations can be obtained for the test data when a_0 ranges from ~ 0.1 to 1 for α values from ~ 1.4 to 4 m^{-1} (Fig. 1).

This model performs well when compared with the *EEMT* model of Pelletier and Rasmussen (2009). The climate-dependent weathering model outperforms the *EEMT* model most noticeably at low soil production rates (Fig. 2). We note that the *EEMT* model does an excellent job of predicting erosion rates based on the Riebe et al.'s (2004) dataset. Residuals of the modelled SPR_{max} also provide some insight into model performance (Fig. 3). While misfits are occasionally large for the silicate weathering model presented here, they are typically randomly distributed across changes in temperature (Fig. 3a), precipitation (Fig. 3b), soil depth (Fig. 3c), and denudation rate (Fig. 3d). This suggests that there is no major bias in the model. However, the model does tend to underfit SPR at high soil depths and high denudation rates. The later tends to support the findings of Heimsath et al. (2012) that SPR_{max} may increase with increasing erosion rates. Gradients in the misfits are apparent in the *EEMT* model. The model tends to underfit at low

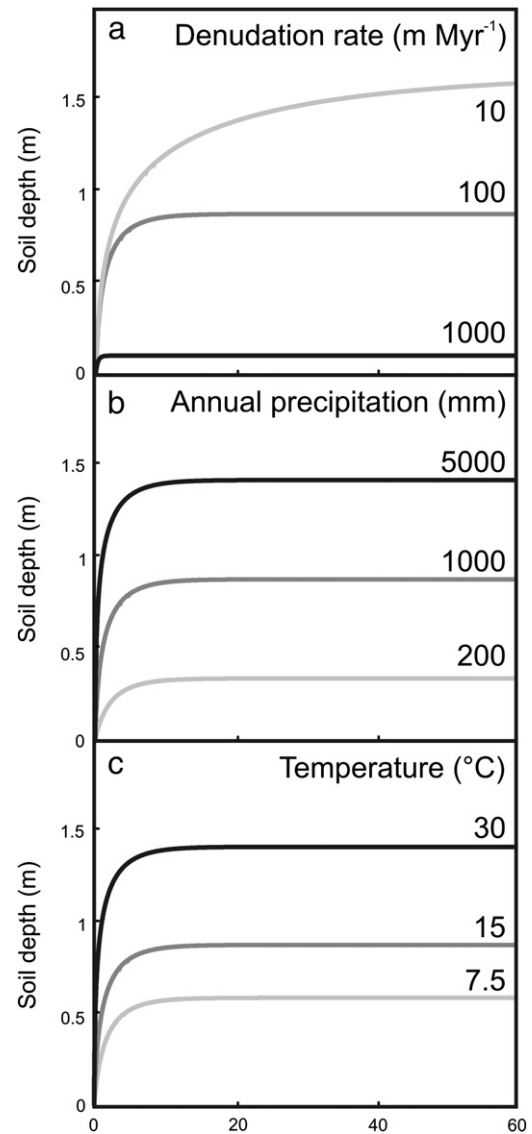


Fig. 4. Approach to steady state for a) 10-fold increase (black line) and decrease (light grey line) of denudation rate from average values (medium grey line), b) 5-fold increase (black line) and decrease (light grey line) of precipitation rate from average values (medium grey line), and c) 2-fold increase (black line) and decrease (light grey line) from average values (medium grey line). Changes which result in soil reduction (i.e., increased denudation or decreased precipitation or temperature) are associated with shorter response times than the opposite changes.

temperatures, high precipitation and high soil depths. However, the dearth of data at high soil depths makes this relationship less robust.

3.2. Climatic and erosional controls on soil production

We first present the results of sensitivity analyses. We use the erosion rate (11 mm ky^{-1}), precipitation rate (800 mm yr^{-1}), and mean temperature (6°C) from the plateau of the Rio Pisco, Peru, as standard values for these tests. Note that for the left hand side of the hump-shaped function, an initial regolith depth of 0.1 m was applied throughout the time transgressive runs, e.g., using Eqs. (8) to (10) in all other cases, and the initial soil depth was 0 . The first test is the effect of a 2-fold increase or decrease of the standard values (Fig. 4). As predicted by theory and existing data (Cox, 1980; Dietrich et al., 1995; Heimsath et al., 1997), steady state regolith thickness increases with decreasing erosion rate, and vice versa (Fig. 4a). The scenario is opposite for precipitation, with regolith becoming thicker with increasing precipitation rate (Fig. 4b). The result at steady state of doubling denudation rate in our model is equivalent to halving the precipitation rate. Interestingly, however, the approach to steady state for these changes is different (Figs. 4 and 5). The response time for a doubling of erosion rate is much shorter than for the equivalent decrease in precipitation rate.

3.3. Response times

We define the response time of the weathering system as the time required to reach 99% of the steady-state regolith thickness, determined iteratively using Eqs. (8) to (10). Variations in both precipitation and denudation result in changes in the response time of the system (Fig. 5). Increased rates are associated with shorter response times and vice

versa. For the case of the exponential function (Fig. 5b, d), a 10-fold increase in denudation rate is associated with an approximately 10-fold decrease in response time (Fig. 5b). Precipitation has a much smaller influence on response time, such that a 10-fold increase in precipitation rate results in an approximately 0.01-fold change in response time (Fig. 5d). For both situations, these relationships hold only up to a threshold, beyond which response times fall to 0. This occurs when the regolith production rate becomes slower than the denudation rate. The definition of response time breaks down at this point as regolith has disappeared from the hillslope. This threshold occurs at high denudation rates and low precipitation rates. Because of this, there is a maximum possible response time with respect to precipitation rate, whereas for denudation rates, the already decreasing response times fall even more rapidly. The hump-shaped function results in slightly lower response times than the exponential model (Fig. 5a, c). The peaks in Fig. 5a, c are due to the effect of the linear portion of the hump-shaped model which increases the response time as the production rate approaches the denudation rate.

3.4. Limits on regolith thickness

Steady state regolith thickness (Eqs. (11) to (13)) exhibits a threshold related to the system response time described above. As denudation rates increase for a given precipitation rate (Fig. 6b), regolith thickness decreases, rapidly approaching zero at a threshold denudation rate. This threshold is higher for higher precipitation rates, which is related to the faster regolith production and longer residence times, where residence time is defined as $H / (dH / dt)$ associated with more precipitation (e.g., Fig. 7b). For the left hand side of the hump-shaped production function, steady state regolith first thickens with increasing denudation

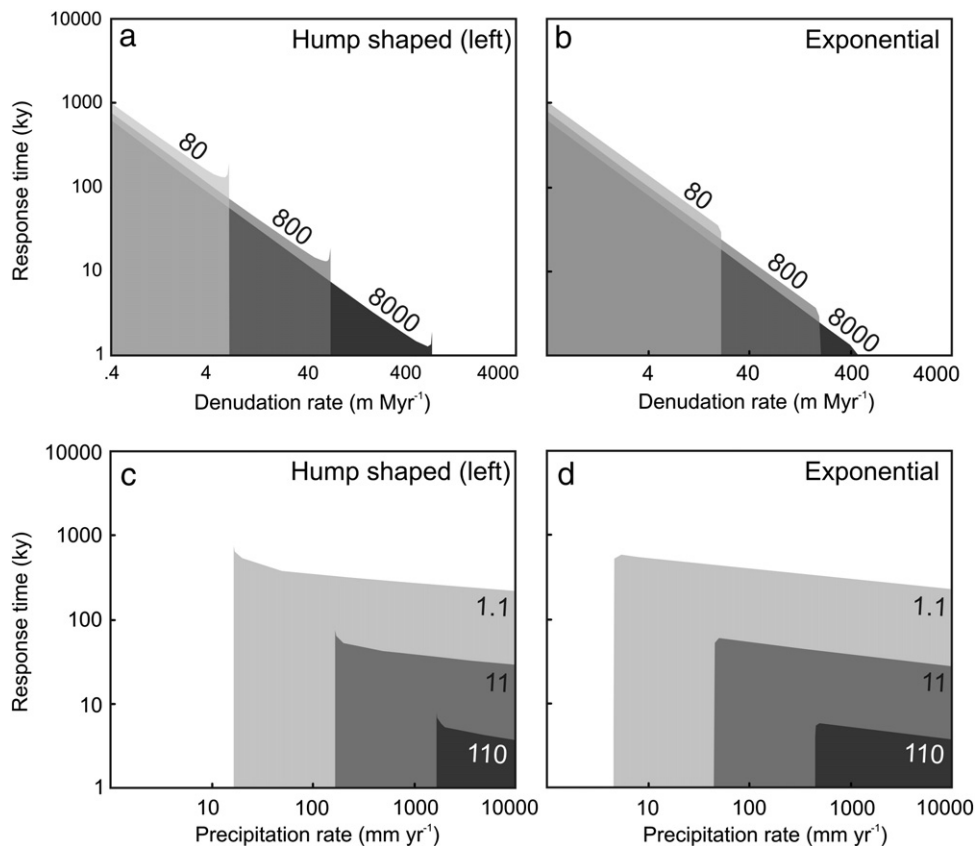


Fig. 5. System response time, defined as the time to reach 99% of the steady state soil thickness, plotted against denudation rate for model precipitation rates (a and b); and precipitation rate for model denudation rates (c and d). Examples are shown for average values from the Rio Pisco soils ($800 \text{ mm annual rainfall}$ and 11 mm yr^{-1} erosion; medium grey), $10\times$ increase ($8000 \text{ mm annual rainfall}$ and 110 mm yr^{-1} erosion; black) and $10\times$ decrease ($80 \text{ mm annual rainfall}$ and 1.1 mm yr^{-1} erosion; light grey) in rates using both the hump shaped (a and c) and exponential (b and d) solutions. Changes in denudation rate have a stronger effect on soil residence time than changes in precipitation rate in the supply limited regime.

rates (Fig. 6a). This is due to the steady state assumption and the positive feedback between production rate and thickness. In general, the hump-shaped production function results in thinner regolith as reported by Pelletier and Rasmussen (2009). Residence times decrease as regolith thins, reaching zero as the cover disappears (Figs. 6 and 7). We also note that these thresholds on regolith sustainability will occur at higher denudation rates if the maximum soil production rate SPR_{max} is also dependent on erosion (Heimsath et al., 2012). To date, no data exist to suggest whether these thresholds will be uniformly shifted or if there is a climate dependence on maximum production rates as well.

4. Discussion

The responses seen here are best considered in the framework of weathering limits. Much of the recent chemical weathering research has focused on the concept of threshold conditions (West et al., 2005; Hren et al., 2007; Dixon et al., 2009; Gabet and Mudd, 2009; Lebedeva et al., 2010; Norton and von Blanckenburg, 2010). In the supply-limited case, the regolith has a long residence time in the weathering zone, and all weatherable materials are consumed (Fig. 7). This is typically associated with thick cover and slow denudation rates. Here, we also note that faster reaction kinetics (through higher temperatures and precipitation rates) can also help push weathering into this state (Fig. 6). Kinetically-limited weathering on the other hand has residence times which are short compared to reaction rates (Fig. 7). Some easily weathered minerals (e.g., biotite and plagioclase feldspar) make it through the entire soil column without being completely reacted. This

situation is associated with thin cover and rapid denudation rates, or likewise, sub-optimum climatic conditions (Fig. 6). A supply limit to weathering explains similar regolith thicknesses at low denudation rates, over a large range of precipitation rates (Fig. 5). In this case, the movement of fresh rock into the weathering zone is much slower than weathering rates such that residence times are very long. Long residence times, as found for supply-limited weathering, result in long response times to climatic or denudation changes. As residence times decrease, the weathering approaches a kinetic limit, and in the extreme case, weathered regolith is removed completely.

Response times decrease for both increasing denudation and precipitation rates. There is, however, a threshold for both cases, which lies towards faster denudation rates and less precipitation. This threshold is also related to the kinetic limit for rock weathering. Faster denudation rates always result in shorter response times, but a maximum response time exists for changes in precipitation rate (Fig. 5). If the denudation rate is held constant, system response time increases with decreasing precipitation (due to slower regolith production rates) until the regolith production rate falls below the denudation rate, at which point weathered regolith disappears completely. An additional complication, recently suggested by Heimsath et al. (2012) is that the maximum regolith production rate may also be dependent on erosion rates such that faster erosion rates yield faster production rates. We do not include erosion in our formulation of maximum regolith production, but note that such a relationship would lead to enhanced regolith thickness in the fastest eroding landscapes, but have little effect in more moderate landscapes.

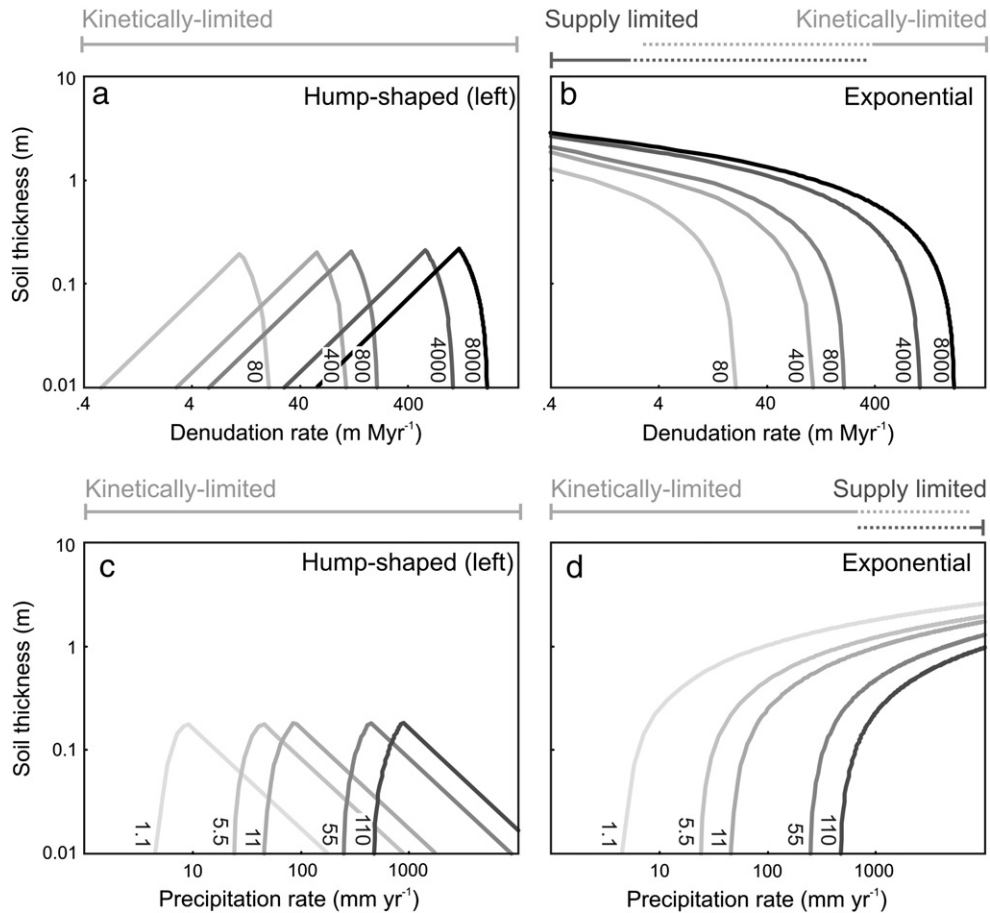


Fig. 6. Variation in steady state soil thickness predicted for variable denudation rates with a given precipitation rate (a and b) and variable precipitation rates with a given denudation rate (c and d). More annual precipitation (4000 and 8000 mm) is designated with darker lines while less annual precipitation (80 and 400 mm) is designated with lighter lines. Likewise, faster erosion (55 and 110 mm yr⁻¹) is designated with darker lines, and slower erosion (1.1 and 5.5 mm yr⁻¹) is designated with lighter lines. Hump shaped solutions are shown on the left and exponential on the right. The approximate boundaries for supply and kinetically-limited weathering are indicated.

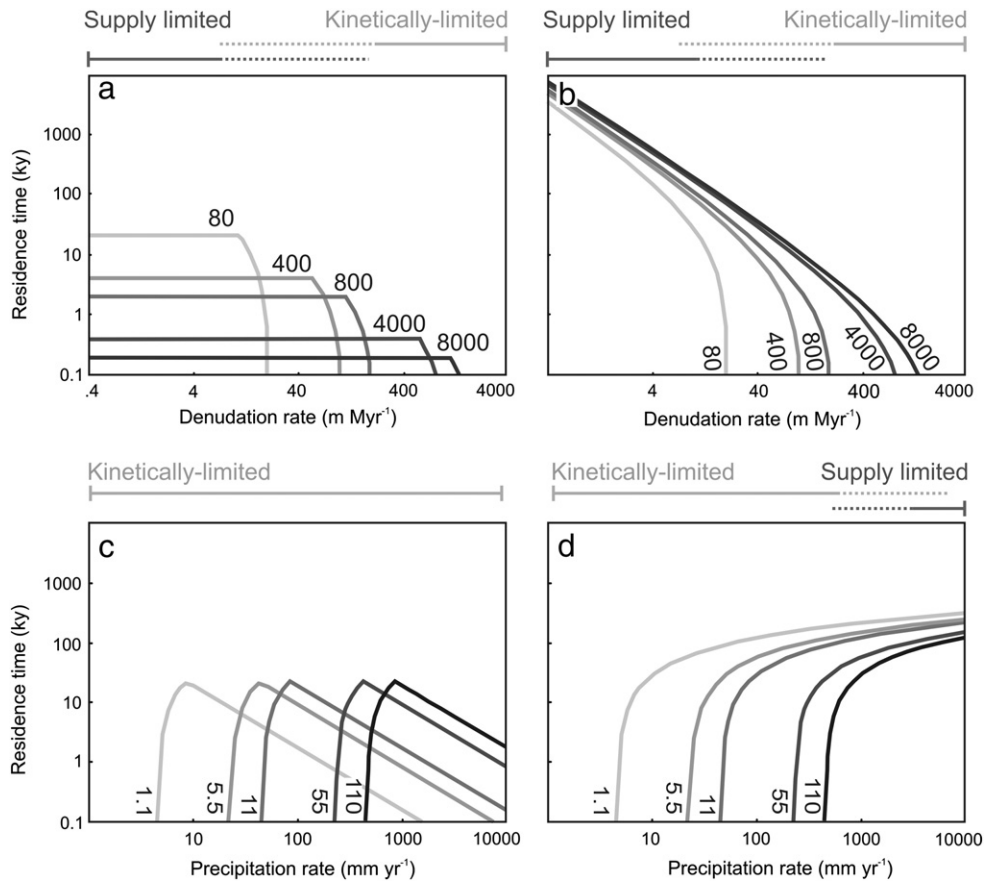


Fig. 7. Residence time of soil plotted against denudation rate for selected precipitation rates (a and b), and precipitation rate for selected denudation rates (c and d). More annual precipitation (4000 and 8000 mm) is designated with darker lines while less annual precipitation (80 and 400 mm) is designated with lighter lines. Likewise, faster erosion (55 and 110 m Myr^{-1}) is designated with darker lines and slower erosion (1.1 and 5.5 m Myr^{-1}) is designated with lighter lines. Hump shaped solutions are shown on the left and exponential on the right. The approximate boundaries for supply and kinetically-limited weathering are indicated.

5. Conclusion

Increasing pressures on global soils require a greater understanding of the processes by which weathered regolith is produced and erodes. An ultimate goal of such research would be a predictive model of soil sustainability under natural forcing parameters. To calibrate such a model, we need more information on the effects of both climate and erosion on weathered regolith production rates. Simple models as presented here can help guide such studies. If one is searching for climate imprints on regolith thickness, it is necessary to go to regions of slow denudation. In turn, denudational controls on regolith thickness can only be determined where production rates are faster than the hill-slope denudation rate, so that regions of high precipitation rates and temperature offer the best possibility for defining empirical relationships between denudation and regolith thickness.

Acknowledgements

The authors would like to thank the coordinators and participants of the 2010 William Smith Meeting of the London Geological Society for input. Comments and discussions with Josh West greatly improved this manuscript. Prof. Takashi Oguchi provided excellent editorial handling. Markus Egli and an anonymous reviewer helped to improve this manuscript. This research was made possible by a post-doctoral grant to KPN from the Swiss National Sciences Foundation (No. 200020-121680) awarded to FS.

References

- Abbühl, L.M., Norton, K.P., Schlunegger, F., Kracht, O., Aldahan, A., Possnert, G., 2010. En Niño forcing on ^{10}Be -based surface denudation rates in the northwestern Peruvian Andes? *Geomorphology* 123, 257–268.
- Ahnert, F., 1967. The role of the equilibrium concept in the interpretation of landforms of fluvial erosion and deposition. In: Macar, P. (Ed.), *L'évolution des versants*. University of Liege, Liege, pp. 23–41.
- Ahnert, F., 1976. Brief description of a comprehensive three-dimensional process-response model of landform development. *Z. Geomorphol. N. F. Suppl.* Bd 25, 29–49.
- Anderson, R.S., 2002. Modeling the tor-dotted crests, bedrock edges, and parabolic profiles of high alpine surfaces of the Wind River Range, Wyoming. *Geomorphology* 46, 35–58.
- Bierman, P.R., Nichols, K.K., 2004. Rock to sediment–slope to sea with Be-10 – rates of landscape change. *Ann. Rev. Earth Planet. Sci.* 32, 215–255.
- Binnie, S.A., Phillips, W.M., Summerfield, M.A., Fifield, L.K., 2007. Tectonic uplift, threshold hillslopes, and denudation rates in a developing mountain range. *Geology* 35, 743–746.
- Carson, M.A., Kirkby, M.J., 1972. *Hillslope Form and Process*. Cambridge University Press, Cambridge.
- Cox, N.J., 1980. On the relationship between bedrock lowering and regolith thickness. *Earth Surf. Process.* 5, 271–274.
- DiBiase, R., Whipple, K.X., Heimsath, A.M., Ouimet, W.B., 2010. Landscape form and millennial erosion rates in the San Gabriel Mountains, CA. *Earth Planet. Sci. Lett.* 289, 134–144.
- Dietrich, W.E., Reiss, R., Hsu, M.-L., Montgomery, D.R., 1995. A process-based model for colluvial soil depth and shallow landsliding using digital elevation data. *Hydro. Processes* 9, 383–400.
- Dietrich, W.E., Bellugi, D., Heimsath, A.M., Roering, J.J., Sklar, L., Stock, J.D., 2003. Geomorphic transport laws for predicting landscape form and dynamics. In: Wilcock, P., Iverson, R. (Eds.), *Prediction in Geomorphology*. American Geophysical Union, Washington, D.C., pp. 103–132.
- Dixon, J.L., von Blanckenburg, F., 2012. Soils as pacemakers and limiters of global silicate weathering. *C.R. Geosci.* 344, 597–609.
- Dixon, J.L., Heimsath, A.M., Anundson, R., 2009. The critical role of climate and saprolite weathering in landscape evolution. *Earth Surf. Process. Landforms* 34, 1507–1521.

- Egli, M., Mirabella, A., Sartori, G., Fitze, P., 2003. Weathering rates as a function of climate: results from a climosequence of the Val Genova (Trentino, Italian Alps). *Geoderma* 111, 99–121.
- Ferrier, K.L., Kirchner, J.W., 2008. Effects of physical erosion on chemical denudation rates: a numerical modeling study of soil-mantled hillslopes. *Earth Planet. Sci. Lett.* 272, 591–599.
- Gabet, E.J., Mudd, S.M., 2009. A theoretical model coupling chemical weathering rates with denudation rates. *Geology* 37, 151–154.
- Gabet, E.J., Mudd, S.M., 2010. Bedrock erosion by root fracture and tree throw: a coupled biogeomorphic model to explore the humped soil production function and the persistence of hillslope soils. *J. Geophys. Res.* 115, F04005 <http://dx.doi.org/10.1029/2009JF001526>.
- Heimsath, A.M., Dietrich, W.E., Nishiizumi, K., Finkel, R.C., 1997. The soil production function and landscape equilibrium. *Nature* 388, 358–361.
- Heimsath, A.M., Chappell, J., Dietrich, W.E., Nishiizumi, K., Finkel, R.C., 2000. Soil production on a retreating escarpment in southeastern Australia. *Geology* 28, 787–790.
- Heimsath, A.M., Dietrich, W.E., Nishiizumi, K., Finkel, R.C., 2001a. Stochastic processes of soil production and transport: erosion rates, topographic variation, and cosmogenic nuclides in the Oregon Coast Range. *Earth Surf. Process. Landforms* 26, 531–552.
- Heimsath, A.M., Chappell, J., Dietrich, W.E., Nishiizumi, K., Finkel, R.C., 2001b. Late Quaternary erosion in southeastern Australia: a field example using cosmogenic nuclides. *Quat. Int.* 83, 169–185.
- Heimsath, A.M., Furbish, D.J., Dietrich, W.E., 2005. The illusion of diffusion: field evidence for depth-dependent sediment transport. *Geology* 33, 949–952.
- Heimsath, A.M., Fink, D., Hancock, G.R., 2009. The 'humped' soil production function: eroding Arnhem Land, Australia. *Earth Surf. Process. Landforms* 34, 1674–1684.
- Heimsath, A.M., DiBiase, R., Whipple, K.X., 2012. Soil production limits and the transition to bedrock-dominated landscapes. *Nat. Geosci.* 1–5.
- Hren, M.T., Hilley, G.E., Chamberlain, C.P., 2007. The relationship between tectonic uplift and chemical weathering rates in the Washington Cascades: field measurements and model predictions. *Am. J. Sci.* 307, 1041–1063.
- Humphreys, G.S., Wilkinson, M.T., 2007. The soil production function: a brief history and its rediscovery. *Geoderma* 139, 73–79.
- Jenny, H., 1941. *Factors of Soil Formation: A System of Quantitative Pedology*. McGraw-Hill, New York.
- Johnson, D.L., Domier, J.E.J., Johnson, D.N., 2005a. Animating the biodynamics of soil thickness using process vector analysis: a dynamic denudation approach to soil formation. *Geomorphology* 67, 23–46.
- Johnson, D.L., Domier, J.E.J., Johnson, D.N., 2005b. Reflections on the nature of soil and its biomantle. *Ann. Assoc. Am. Geogr.* 95, 11–31.
- Kober, F., Schlunegger, F., Zeilinger, G., Schneider, H. (Eds.), 2006. *Surface Uplift and Climate Change: The Geomorphic Evolution of the Western Escarpment of the Andes of Northern Chile between the Miocene and Present*. Tectonics, Climate, and Landscape Evolution, Geological Society of America Special Paper, 398. Geological Society of America, Boulder.
- Lebedeva, M.I., Fletcher, R.C., Brantley, S.L., 2010. A mathematical model for steady-state regolith production at constant erosion rate. *Earth Surf. Process. Landforms* 35, 508–524.
- Matmon, A., Bierman, P., Enzel, Y., 2002. Pattern and tempo of great escarpment erosion. *Geology* 30, 1135–1138.
- Minasny, B., McBratney, A.B., Salvador-Blanes, S., 2008. Quantitative models for pedogenesis — a review. *Geoderma* 144, 140–157.
- Norton, K.P., von Blanckenburg, F., 2010. Silicate weathering of soil-mantled slopes in an active Alpine landscape. *Geochim. Cosmochim. Acta* 74, 5243–5258.
- Norton, K.P., von Blanckenburg, F., Schlunegger, F., Schwab, M., Kubik, P.W., 2008. Cosmogenic nuclide-based investigation of spatial erosion and hillslope channel coupling in the transient foreland of the Swiss Alps. *Geomorphology* 95, 474–486.
- Norton, K.P., von Blanckenburg, F., Kubik, P.W., 2010. Cosmogenic nuclide-derived rates of diffusive and episodic erosion in the glacially sculpted upper Rhone Valley, Swiss Alps. *Earth Surf. Process. Landforms* 35, 651–662.
- Pelletier, J.D., Rasmussen, C., 2009. Quantifying the climatic and tectonic controls on hillslope steepness and erosion rate. *Lithosphere* 1, 73–80.
- Rasmussen, C., Tabor, N.J., 2007. Applying a quantitative pedogenic energy model across a range of environmental gradients. *Soil Sci. Soc. Am. J.* 71, 1719–1729.
- Rasmussen, C., Brantley, S.L., Richter, D., Blum, A.E., Dixon, J.L., White, A.F., 2011. Strong climate control on plagioclase weathering in granitic terrain. *Earth Planet. Sci. Lett.* 301, 521–530.
- Riebe, C.S., Kirchner, J.W., Granger, D.E., Finkel, R.C., 2001. Strong tectonic and weak climatic control of long-term chemical weathering rates. *Geology* 29, 511–514.
- Riebe, C.S., Kirchner, J.W., Finkel, R.C., 2004. Erosional and climatic effects on long-term chemical weathering rates in granitic landscapes spanning diverse climate regimes. *Earth Planet. Sci. Lett.* 224, 547–562.
- Roering, J.J., Kirchner, J.W., Dietrich, W.E., 1999. Evidence for non-linear, diffusive sediment transport on hillslopes and implications for landscape morphology. *Water Resour. Res.* 35, 853–870.
- Savi, S., Norton, K.P., Picotti, V., Brardinoni, F., Akcar, N., Kubik, P.W., Delunel, R., Schlunegger, F., 2013. Effects of sediment mixing on ¹⁰Be concentrations in the Zielbach catchment, central-eastern Italian Alps. *Quat. Geochronol.* <http://dx.doi.org/10.1016/j.quageo.2013.01.006> (in press).
- Tucker, G.E., Hancock, G.R., 2010. Modelling landscape evolution. *Earth Surf. Process. Landforms* 35, 28–50.
- Tucker, G.E., Slingerland, R.L., 1994. Erosional dynamics, flexural isostasy, and long-lived escarpments: a numerical modeling study. *J. Geophys. Res. B Solid Earth Planets* 99, 12,229–12,243.
- Tucker, G.E., Slingerland, R., 1997. Drainage basin responses to climate change. *Water Resour. Res.* 33, 2031–2047.
- Velbel, M.A., 1993. Temperature-dependence of silicate weathering in nature — how strong a negative feedback on long-term accumulation of atmospheric CO₂ and global greenhouse warming. *Geology* 21, 1059–1062.
- Volobuyev, V.R., 1974. Main concepts of soil ecology. *Geoderma* 12, 27–33.
- von Blanckenburg, F., 2006. The control mechanisms of erosion and weathering at basin scale from cosmogenic nuclides in river sediment. *Earth Planet. Sci. Lett.* 242, 223–239.
- West, A.J., Galy, A., Bickle, M., 2005. Tectonic and climatic controls on silicate weathering. *Earth Planet. Sci. Lett.* 235, 211–228.
- White, A.F., Blum, A.E., 1995. Effects of climate on chemical weathering in watersheds. *Geochim. Cosmochim. Acta* 59, 1729–1747.
- Williams, J.Z., Bandsra, J.Z., Pollard, D., Brantley, S.L., 2010. The temperature dependence of feldspar dissolution determined using a coupled weathering–climate model for Holocene-aged loess soils. *Geoderma* 156, 11–19.